Temperature Variability in Northeast China over the Past Two Millennia and Linkages with the Arctic Oscillation

Nan Zhan[1,2], Qi Li[3], Manman Xie[1], Ruilin Wen[3], Luo Wang[3], Ruixia Hao[2], Chunqing Sun[3], Guoping Zhang[4], Qing Sun[1]*, and Guoqiang Chu[3*]

[1] National Research Center for Geoanalysis, Key Laboratory of Eco-Geochemistry, Ministry of Natural Resources, Beijing 100037, China

[2]School of Earth and Space Sciences, Peking University, Beijing 100871, China

[3]Institute of Geology and Geophysics, Chinese Academy of Sciences, Beijing 100029, China

[4]CMA Public Meteorological Service Center, Beijing 100080, China

Corresponding author: Qing Sun (sunqing1616@yahoo.com), Guoqiang Chu (chuguoqiang@mail.iggcas.ac.cn)

Key Points:

- BrGDGTs can be used to reconstruct the month-above-freezing temperatures in Northeast China for the past two millennia
- The reconstructed temperature time series exhibited distinct quasi-periodicities of 55-57 and 66-67 years at a 99% significance level
- Regional temperature variability may be primarily influenced by the Arctic Oscillation, North Atlantic Oscillation, and solar activity

Abstract

Temperature reconstruction over the past two millennia has created a crucial database for global networks and for evaluating and predicting global climate change. Here, we present a high-resolution (~5-25 years) temperature reconstruction over the past 2000 years using branched glycerol dialkyl glycerol tetraethers (brGDGTs) from laminated sediments in a crater lake located in Northeast China. The brGDGT-derived proxies accurately represented the month-above-freezing temperatures (MAFT) within our study region. Our temperature reconstruction exhibited distinct decadal-to-centennial variability and showed rough correspondence with the AO/NAO index and solar activity. Furthermore, the spectral analysis identified two quasi-periodicities of 55-57 and 66-67 years within the MAFTs time series at a 99% confidence level, suggesting possible associations with solar activity. These findings imply that long-term temperature variability in Northeast China is mainly regulated by a combination of the AO, NAO, and solar activity.

Plain Language Summary

Paleotemperature reconstruction is crucial for understanding and predicting global climate change. In this study, we quantitatively reconstructed temperatures over the past 2000 years using brGDGTs, a group of lipid biomarkers found in the laminated sediments of Lake Shuanggoushan, a small crater lake in Northeast China. The reconstructed temperatures were confirmed with meteorological data and other paleotemperature records, indicating that they accurately represented the month-above-freezing temperatures in the study region. We observed decadal-to-centennial fluctuations in our temperature reconstruction, which roughly corresponded to the AO/NAO index and solar activity within the range of dating uncertainty. The spectral analysis identified two quasi-periodicities of 55-57 and 66-67 years, which may be related to solar activity. These findings suggest that long-term temperature variability in our study region is influenced by the combined effects of the AO, NAO, and solar activity. Overall, this study provides valuable insights into the temperature evolution and climate-driving mechanisms in Northeast China over the past two millennia.

1 Introduction

Paleotemperature reconstruction is an important way to comprehend modern climate and predict future climate. However, only a few high-resolution temperature records exist with continuous coverage and absolute dating over the past two millennia in Northeast China (Ge et al., 2013; Ljungqvist, 2009; Mann et al., 2008).

Temperature variability in Northeast China is influenced by various factors, including internal climate variability (atmosphere-ocean circulation), external natural forces (solar irradiance and volcanic activity), and anthropogenic activities (Chu et al., 2011; Ge et al., 2013; He et al., 2017). The Arctic Oscillation (AO) is the leading driver of large-scale atmospheric circulation variability over the Northern Hemisphere mid-to-high latitudes and plays an important role in regulating Eurasian temperature variability (He et al., 2017; Thompson & Wallace, 1998). On an interannual timescale, observational evidence has shown that the positive (negative) phase of the winter/spring AO generally leads to warmer (colder) climates in East Asia (Gong et al., 2011; Liu & Ding, 2007). The Siberian High and polar vortex may serve as a bridge for interaction between

the AO and cold waves over East Asia (Park et al., 2011; Woo et al., 2012). During a positive AO phase, a strong mid-latitude jet stream steers storms northward, reducing cold air outbreaks in the mid-latitudes and resulting in warmer temperatures, and vice versa (Chen & Zhou, 2012; He et al., 2017; Liu & Ding, 2007). On decadal to longer timescales, however, the long-term behavior of the AO remains unclear. Therefore, a comprehensive understanding of the AO's long-term variability and its impact on temperature is imperative.

Branched glycerol dialkyl glycerol tetraethers (brGDGTs) are bacterial membrane lipids that are ubiquitous in diverse geological archives, including soils, peats, stalagmites, and lake sediments (Schouten et al., 2013). They have been extensively employed as paleothermometers in quantitative continental paleotemperature studies due to the strong relationships between their relative abundances and environmental temperature (Inglis et al., 2022; Schouten et al., 2013). However, current brGDGTs calibrations still rely on empirical correlations between the relative brGDGT abundance and temperatures due to a limited understanding of their biological origin (Chen et al., 2022; Halamka et al., 2021). Considerable efforts have been made to improve the accuracy of brGDGTs-based temperature proxies, which involve removing interfering components (De Jonge et al., 2014), refining datasets for specific environments such as soils, lakes, and peat (Naafs et al., 2017; Véquaud et al., 2022), and establishing globally- or regionally-specific calibrations (Feng et al., 2019; Martínez-Sosa et al., 2021; Raberg et al., 2021; Zhao et al., 2023). Despite these advances, the use of these proxies in lacustrine systems is still limited due to an incomplete understanding of their origin, seasonal production, and transportation (Loomis et al., 2014; Miller et al., 2018; Zhu et al., 2021).

Here, we present a quantitative temperature reconstruction over the past two millennia based on the brGDGTs from laminated sediments of Lake Shuanggoushan in Northeast China. Our reconstruction provides a long-term temperature variability at a temporal resolution of ~5-25 years, enabling us to investigate the temperature-driving factors and the relationship between temperature variability and the AO behavior.

2 Materials and Methods

2.1 Study Site

Lake Shuanggoushan (120º44′E; 47º28′N) is a small crater lake situated in northeastern China in the Arxan-Chaihe volcanic field of the Greater Khingan Mountains (Figure 1). It has a surface area of ~0.12 km^2 and a maximum depth of 9.2 m. The lake is surrounded by dense forests and has no inflows or outflows. Located on the northern boundary of the East Asian Monsoon, the lake is sensitive to temperature, resulting in warm and rainy weather during summer and cold and dry conditions in winter. Typically, the lake freezes between late October and late April, forming an ice sheet of ~1.2 m thick.

The Arxan station, situated ~70 km from Lake Shuanggoushan, has collected meteorological data since 1954. Although the weather station is the closest one to the lake, its elevation (997 m above sea level) is 300 meters lower than that of the lake (1290 m.a.s.l.). Therefore, meteorological data is adjusted using a lapse rate of 0.6 ℃/100 m to correct lake temperatures, including adjustments for Mean Annual Air Temperature (MAAT), Months-Above-Freezing Temperature (MAFT, May-October), and Mean Summer Air Temperature (MSAT, June-August).

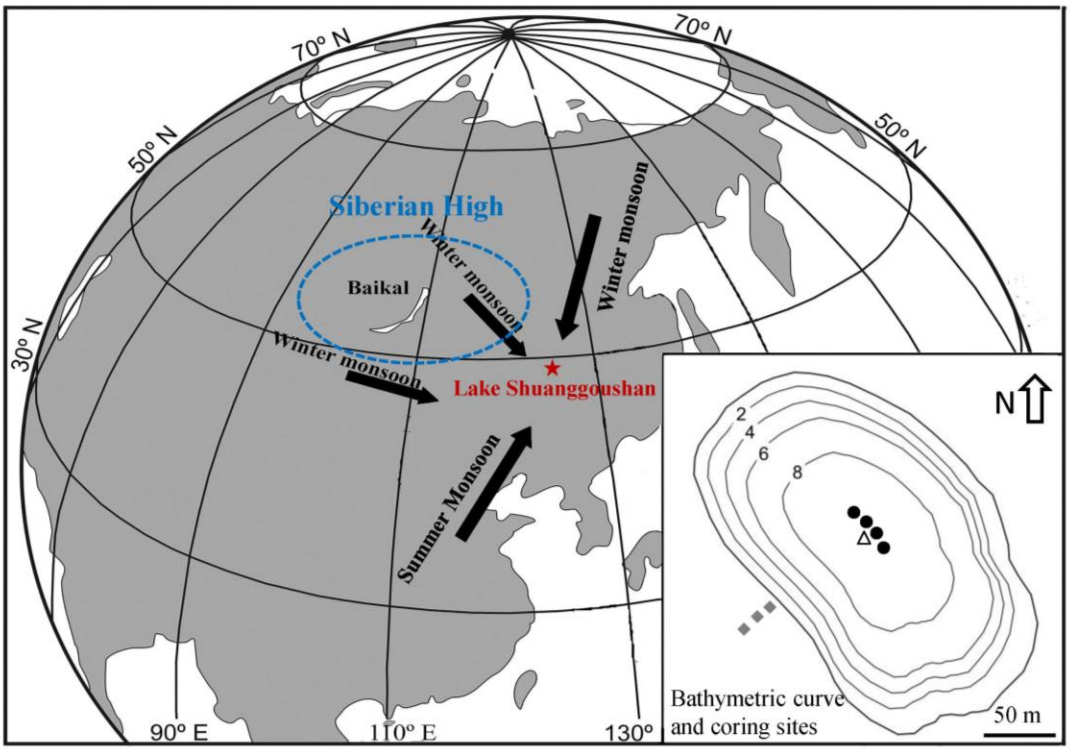

Figure 1. Location of the Lake Shuanggoushan (red star), which is situated at the northern boundary of the East Asian Monsoon. The black arrows indicate the dominant direction of the Asian winter and summer monsoon, and the blue circle indicates Siberian High. The inset shows the lake bathymetry photo and sampling sites for sediment cores (black circle), catchment soils (grey diamond), and lake water SPM samples (white triangle).

2.2 Sediment Cores and Chronology

A series of gravity cores were retrieved from Lake Shuanggoushan in 2020 and 2021 (Figure 1). Two cores, SG-2020-B and SG-2021-B1, were selected for this study and split in half lengthwise for investigation. One-half of each core was used for GDGT analysis, and the other half was prepared for thin sections. The upper sediment cores (0-80 cm) were sectioned at 0.5 cm intervals for GDGT analysis, while the lower part (80-95 cm) was sectioned at 1 cm intervals. A total of 175 lake sediment samples were obtained from the sediment cores that covered the past 2000 years. Additionally, three surface soil samples were collected from the southwest slope of the lake catchment area, and three suspended particulate matter (SPM) samples were collected by filtering 10 L of lake water through a 0.45 μm filter. All samples were frozen at -20 ℃ in the laboratory prior to analysis.

Radiometric dating (^{137}Cs, ^{210}Pb, and ^{226}Ra) was performed using gamma spectrometry with a low-background well-type germanium detector (EGPC 100P-15R, Eurisys Mesures, France). Each sample was packed in a 15 mm diameter polyethylene tube and stored in sealed containers for three weeks to allow for radioactive equilibration. Radiocarbon ages were determined using accelerator mass spectrometry at the Beta Analytic Radiocarbon Dating Laboratory (USA) and then converted to calendar years using the IntCal20 calibration dataset (Reimer et al., 2020, Supplementary Table S1).

Varves were identified from thin sections and counted using a polarizing microscope. Sediment slabs (60 mm × 20 mm × 10 mm) were cut from sediment cores, then shock-frozen, vacuum-dried, penetrated with epoxy resin, and sliced into thin sections marked with centimeter scales using a pencil. Millimeter-scale laminations were identified and counted from the thin sections at various magnifications under the microscope (Supplementary Figure S2).

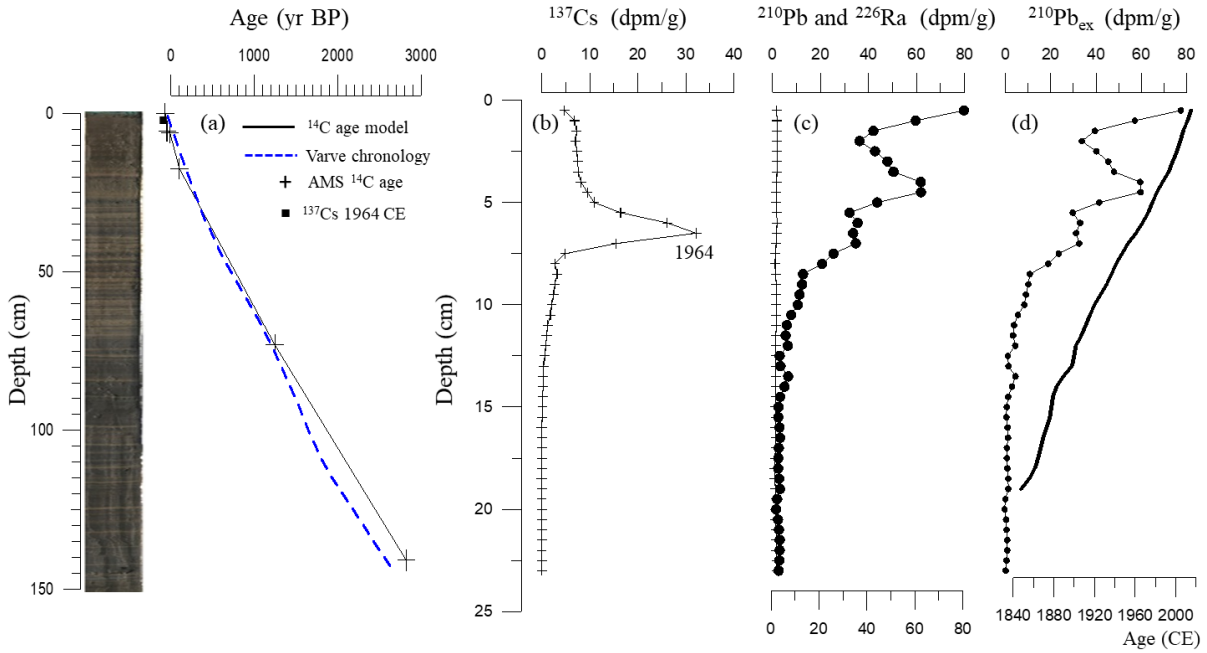

Figure 2. Age-depth model for sediment cores from Lake Shuanggoushan. Chronologies were derived from ^{137}Cs, ^{210}Pb, ^{14}C dating, and valves-counting in the sediment.

2.3 GDGTs Analysis

Before extraction, the lake sediment and soil samples were freeze-dried, homogenized, and weighed accurately to ~1.0 g, while the SPM samples were cut into small fragments. All samples were extracted using an Accelerated Solvent Extractor (Dionex 350, Thermo Scientific, USA) with a mixture of dichloromethane (DCM): methanol (MeOH, 9:1, v/v) at 120 ℃ and 1500 psi for three cycles. The lipid extract was separated into nonpolar and polar fractions via an activated Al_2O_3 column (30 × 4 mm i.d.) with hexane: DCM (9:1, v/v) and DCM: MeOH (1:1, v/v), respectively. The polar fraction, which contained GDGTs, was dried under nitrogen steam, dissolved in an n-hexane: isopropanol (98:2, v/v) mixture, and filtered through a 0.45 μm PTFE filter with the addition of the internal standard (C_{46}-GTGT) before analysis.

The brGDGTs analysis was performed by high-performance liquid chromatography-atmospheric pressure chemical ionization-mass spectrometry (HPLC-APCI-MS, AB Sciex API4000). Separation of 5-, 6-, and 7-methyl brGDGTs was achieved using two BEH HILIC columns (150 mm × 2.1 mm × 1.7 μm, Waters, USA) and one Hypersil GOLD silica column (150 mm × 2.1 mm × 1.9 μm, Thermo Finnigan, USA) in sequence, all maintained at 40 ℃. The solvent composition was initially held at 94% hexane (A) and 6% isopropanol (B) for 80 min, followed by an increase to 25% B for 20 min, which was maintained for 5 min, then decreased to 0% B for 3 min and finally re-equilibrated back to 6%B for 15 min. The flow rate remained constant at 0.2 mL/min. Ion scanning was performed in the selected ion monitoring mode via $[M+H]^+$ at m/z 1050,

1048, 1046, 1036, 1034, 1032, 1022, 1020, 1018, and 744 for C_{46} internal standard. The peak area of each brGDGT was compared with C_{46}-GTGT for quantification. Duplicate sample analysis showed that the analytical error for each brGDGT was less than 5%.

2.4 BrGDGT-related Temperature Proxies and Calibrations

The relative abundance of brGDGTs are represented by Roman numerals I, II, and III, and their structures are shown in Supplementary Figure S1. BrGDGTs-based proxies, such as MBT' (Peterse et al., 2012), MBT'$_{5ME}$ (De Jonge et al., 2014), MBT_m (Zink et al., 2016), and CBT (Weijers et al., 2007) is used to quantify the relative degree of methylation and cyclization of these compounds.

$$CBT = -\log[(Ib+IIb)/(Ia+IIa)] \quad (1)$$

$$MBT' = (Ia+Ib+Ic)/(Ia+Ib+Ic+IIa+IIa'+IIb+IIc+IIIa+IIIa') \quad (2)$$

$$MBT'_{5ME} = (Ia+Ib+Ic)/(Ia+Ib+Ic+IIa+IIb+IIc+IIIa) \quad (3)$$

$$MBT'_{6ME} = (Ia+Ib+Ic)/(Ia+Ib+Ic+IIa'+IIb'+IIc'+IIIa') \quad (4)$$

$$MBT_m = (IIIa+IIIb+IIIc)/(Ia+Ib+Ic+IIa+IIb+IIc+IIIa+IIIb+IIIc) \quad (5)$$

To estimate the paleotemperatures of Lake Shuanggoushan, we utilized various lake-specific calibrations, including regional and global, as described in Equation 6-12:

$$MAAT = 6.803-7.062 \times CBT+37.09 \times MBT \quad (6)$$

$$MAFT = (MBT'_{5ME} - 0.075)/0.03 \quad (7)$$

$$MAFT = 1.44+15.88 \times f(Ia)+66.92 \times f(Ib)+8.33 \times f(IIa')+7.02 \times f(IIIa') \quad (8)$$

$$MAFT = 30.4 \times MBT_m - 0.5 \quad (9)$$

$$MAFT = 13.116-7.998 \times CBT+27.752 \times MBT \quad (10)$$

$$MSAT = -28.274 \times MBT_m+19.993 \quad (11)$$

$$MSAT = 18.72 \times MBT'_{6ME} - 5.92 \quad (12)$$

The fractional abundance of each brGDGT compound, $f(xi)$, was calculated as follows:
$f(xi) = xi/(Ia+Ib+Ic+IIa+IIb+IIc+IIIa+IIIb+IIIc+IIa'+IIb'+IIc'+IIIa'+IIIb'+IIIc')$
where xi is any one of the brGDGTs.

3 Results and Discussion

3.1 Chronology

Figure 2 shows the ^{137}Cs, ^{210}Pb, and ^{226}Ra activities versus depth. Maximum ^{137}Cs activity occurred at a depth of 6.5 cm, which serves as a time marker for the period of atmospheric nuclear weapons testing in 1963-1964 CE (Figure 2b). The unsupported activity of ^{210}Pb ($^{210}Pb_{un}$), calculated by subtracting the ^{226}Ra activity, decreased exponentially with depth and reached zero below 12 cm. The sedimentary ages and sedimentation rates of the upper interval (0-17.5 cm) were established using the CRS model based on ^{210}Pb and ^{137}Cs (Appleby et al., 1986; Sanchez-Cabeza & Ruiz-Fernández, 2012). The chronology for sediment cores below 17.5 cm was based on linear interpolation of AMS^{14}C data obtained from three plant fragments at different depths (Figure 2a, Supplementary Table S2).

Organic-clastic varves, which consisted of light and dark laminas, were observed in the sediment cores (Supplementary Figure S2). The dark organic layer was mainly composed of diatoms and organic remains, whereas the light layer was mainly composed of clay and silt under polarized light. However, varves were absent or poorly developed in the upper part and some intervals. We estimated the number based on the upper or lower centimeter varves in such cases. Overall, the varve ages were in good agreement with the AMS^{14}C dating results (Figure 2a).

3.2 Distribution and Source of brGDGTs in Lake Shuanggoushan

Of the 185 lake sediment samples, pentamethylated (39.3%) and hexamethylated brGDGTs (38.3%) were the most prevalent, whereas tetramethylated brGDGTs (22.4%) were less abundant (Figure 3). All samples contained 5- and 6-methyl brGDGTs regioisomers, but only a small fraction (<1%) of samples contained the 7-methyl isomers. The distribution of brGDGTs in Lake Shuanggoushan was different from global and tropical lakes (Mat ńez-Sosa et al., 2021; Russell et al., 2018) but more similar to lakes located in mid-to-high latitudes (Liang et al., 2022).

Identifying the source of brGDGTs in lacustrine sediments is crucial for accurate temperature reconstruction. This study compared the distribution of brGDGTs in catchment soils, SPM, and lake sediments from Lake Shuanggoushan (Figure S4). The relative abundance of brGDGTs in lake sediments and SPM was similar but was significantly different from the catchment soil results, especially for the major components Ia, IIa, IIa', IIIa, and IIIa'. The lake sediment and SPM samples exhibited nearly twice the abundance of IIIa compared to the catchment soils. In contrast, the abundances of Ia and IIa in the lake sediments and the SPM were only half that of the catchment soils. Such similarities between lake sediment and SPM samples suggest that most of the brGDGTs in the lake are produced in situ. The ∑IIIa/∑IIa ratio, ranging from 0.87 to 1.46, with only 12 out of 185 sediment samples having ratios less than 0.92, further confirmed that the brGDGTs primarily originate from the lake (Xiao et al., 2016). Moreover, the CBT/MBT$_m$ ratios, ranging from 1.98 to 4.79, also indicated that the lacustrine brGDGTs are primarily of local origin, as this ratio is typically higher in soils (>7) than in lakes (Zink et al., 2016). These findings indicate that the brGDGTs in the lake sediments are mainly from in situ lake production, with a negligible contribution from the surrounding soils.

3.3 BrGDGTs-derived Temperature in Lake Shuanggoushan

Since Lake Shuanggoushan is a small closed lake and the brGDGTs in lake sediment are mainly produced within the lake, we used lacustrine calibrations (Equations 6-12), including regional and global calibrations, to reconstruct temperatures of the past 60 years. Moreover, we compared the reconstructed temperatures (i.e., MAAT, MAFT, and MSAT) with instrumental data from the Arxan meteorological station to verify the impact of seasonality and selected the most appropriate calibration for Lake Shuanggoushan.

After applying the calibrations for global lakes, the reconstructed MAFTs using Equation 7 (Matinez-Sosa et al. 2021) were underestimated by an average of 6.7 ℃ when compared to the instrumental records. Similarly, when compared to the temperature records from the weather station, the reconstructed MAFTs generated by Equations 8 (Zhao et al. 2023) and 9 (Raberg et al. 2021) were underestimated by 5.8 ℃ and 5.4 ℃, respectively. Applying mid-latitude regional calibrations, such as Equations 11 (Zink et al. 2016) and 12 (Liang et al. 2022), resulted in reconstructed MSATs that were lower than the instrumental temperatures by 2.2 ℃ and 1.0 ℃, respectively (Supplementary Table S2). Furthermore, our findings indicate that MAFTs

outperformed MAATs in brGDGT temperature reconstructions. The reconstructed MAATs, using Equation 6 (Sun et al., 2011), were overestimated by an average of 10.3 ℃ compared to the actual temperatures. However, the reconstructed MAFTs, calculated using the warm-season calibration Equation 10 (Sun et al., 2011), deviated only by 1.6 ℃ from the instrument records (Supplementary Table S2).

The lacustrine calibrations revealed that Equation 10 yielded the most accurate and precise reconstructions in terms of both temperature difference and correlation ($r=0.86$, $p<0.001$, Supplementary Figure S5). Therefore, it was selected as the most appropriate calibration for the subsequent paleotemperature reconstruction of Lake Shuanggoushan. Additionally, the brGDGT-derived temperatures in our study region reflected warm-season temperature signals rather than annual temperatures or summer temperatures, which is consistent with previous observations of warm-season bias in brGDGT-estimated temperatures in shallow lakes at mid-to-high latitudes (Cao et al., 2020; Loomis et al., 2014; Zhu et al., 2021).

3.4 Temperature Reconstruction over the Past Two Millennia

Figure 3a shows the brGDGT-derived temperature time series in Lake Shuanggoushan over the past two millennia. The reconstructed MAFTs display notable decadal-to-multidecadal fluctuations ranging between 10.0 ℃ and 16.7 ℃, with an average of 12.5 ℃. From 400 to 700 CE, a cold period was known as the 'Dark Age Cold Periods' (DACP), recorded in Europe, North America, and the China/Tibetan Plateau (Helama et al., 2017). From 700 CE to 1300 CE, the 'Medieval Warm Period' (MWP) was characterized by warm temperatures, with an average of 12.8 ℃ and the warmest period during the MWP occurred around 730 CE, with a maximum MAFT of 16.7 ℃. After the beginning of the 'Little Ice Age' (LIA, 1300-1850 CE), the climate underwent a long-term cooling trend. Several rapid cold events occurred during the LIA, including notable cold spells in the 1380s, 1490s, and 1550s, with a temperature drop rate of over 0.5 ℃/10year. The temperatures have steadily increased since 1970 CE but have not surpassed the high temperatures during the MWP.

We then compared our temperature reconstruction with other paleotemperature records from China, neighboring areas, and the Northern Hemisphere. The focus was on the general pattern of temperature variability because different temperature proxies, reconstruction approaches, and chronological uncertainties can lead to varied reconstruction results. Temperature records in Northeast China exhibited similar multi-decadal fluctuations but with temperature amplitudes that were less than half of those in brGDGTs records (Figure 3b, Ge et al., 2013). Moreover, the alkenones-based growing season temperatures at Lake Sihailongwan, which is located near our study region, showed similar variations over the past 1600 years (Figure 3c). However, variations in temperature amplitudes were occasionally observed. For example, during the cold event around 1260 CE, alkenone records showed a significant cooling of up to 5 ℃, whereas brGDGTs records only showed a modest cooling of 1.5 ℃. The tree ring-based summer temperatures in the Northern Hemisphere (Figure 3d; Büntgen et al., 2021) demonstrated comparable fluctuations to our reconstruction, including cool conditions in the 620s, 890s, 1540s, and 1810s, as well as warm periods in the 5th century and the MWP. The above comparison results demonstrate consistent variations across all reconstructions, regardless of the dating uncertainties.

We further note that severe cold spells or sudden cooling during warm seasons coincided with transitions in several agricultural Chinese dynasties, such as the Tang (907 CE), Liao (1125), Southern Song (1279 CE), and Ming (1644 CE) dynasties (Figure 5). This observation is consistent with previous studies that have suggested successive cold growing seasons can result in food

shortages, famine, economic decline, and social unrest, ultimately leading to dynasty collapse (Büntgen et al., 2020; Liang et al., 2022; Zhang et al., 2010;). We found that the Mongol conquest (1206 CE), which ended with the downfall of the Southern Song, as well as the Manchu conquest of China and the overthrow of the Ming dynasty (1580-1650 CE), all coincided with intervals of anomalously cold growing seasons. Conversely, mild growing seasons, such as the Kaiyuan Flourishing Age (712-741 CE) and the High-Qing period (1680-1795 CE), were associated with societal prosperity and political stability. This evidence presented in our reconstruction further proves that temperature variability has played a crucial role in Chinese societal transitions over the past 2000 years.

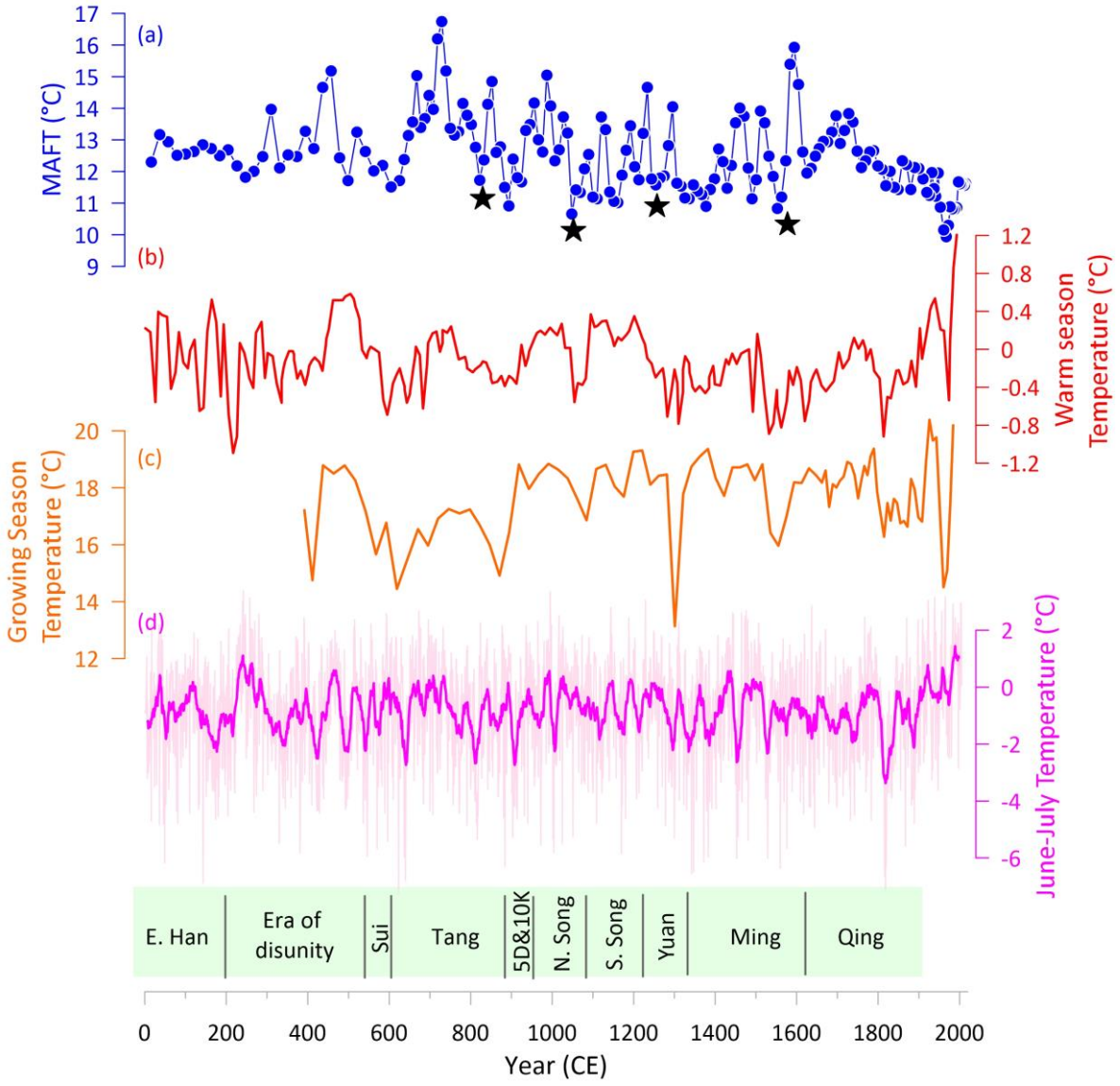

Figure 3. Warm season temperature reconstructions over the past two millennia. (a) brGDGT-based MAFTs from Lake Shuanggoushan (this study); (b) Reconstructed warm season temperature in Northeast China from historical documents and proxy data (red line) (Ge et al., 2013); (c) Alkenone-based temperatures during the growing season in Lake Sihailongwan, Northeast China (orange line) (Chu et al., 2011); (d) Tree-ring-based June-July temperatures in the Northern Hemisphere (pink line) with a 15-year running average (magenta line) (35°-73°N, Büntgen et al.,

2021). Chinese dynasties are indicated at the bottom, and black stars indicate the ends of the Tang, Liao, Southern Song, and Ming dynasties.

3.5 Possible Forcings of Temperature Variability in Northeast China

The AO is considered the dominant factor explaining temperature variations over Eurasia (Chu et al., 2008; He et al., 2017). A comparative analysis of metrological temperatures and AO indices from 1955 to 2014 CE indicated that the AO significantly impacted the interannual temperature variability in our study region (Supplementary Figure S6). The correlation between MAFTs and the AO index was found to be weak ($r=0.25$). Conversely, a strong correlation ($r=0.63$, $p<0.001$) was observed between MAATs and the AO index, while an even stronger correlation ($r=0.65$, $p<0.001$) was identified between winter-spring temperatures (November-April) and the AO index, which is consistent with previous research (Yao et al., 2023). Over the past 2000 years, the temperature trends and variability of MAFTs in Lake Shuanggoushan were also similar to the AO index derived from proxy data (Figures 4b and 4c). Other atmospheric teleconnection patterns, such as the North Atlantic Oscillation (NAO), may also influence the temperature variability in our study region (Knudsen et al., 2011). We found that the proxy-derived NAO index was in relatively good agreement with the temperature reconstruction trends and variability (Figures 4d and 4e). Specifically, when the AO/NAO was in its positive phase, temperatures in the study region were higher, and vice versa. Therefore, it suggests that AO/NAO-like atmospheric variability has influenced the multidecadal temperature variations for the past two millennia.

Solar activity is believed to significantly influence the Earth's surface air temperature and large-scale atmospheric circulation (Soon et al., 2015; Tourpali et al., 2005). Several studies have suggested that solar activity is also a major driving factor for the AO (Chen & Zhou, 2012; Huth et al., 2007; Qu et al., 2014; Veretenenko & Ogurtsov, 2019). Through spectral analysis, we identified two quasi-periodicities (55-57, 66-67 years) at a 99% confidence level and four quasi-periodicities (30, 35-36, 46-47, and 55-58 years) at a 95% confidence level in the temperature fluctuations in our study area over the past two millennia (Supplementary Figure S7). The 55-57 and 66-67-yr periodic oscillations may be related to solar activity, as they are similar to the ~60-yr solar cycle or five times the 11-yr sunspot cycle. The temperature variations and solar activity patterns are similar when the AO/NAO and solar activity trends align (Figure 4). A recent study also found a significant correlation between reconstructed temperature and solar variability in the Schwabe solar cycle and the ~60 and ~90-year spectral window (Land et al., 2020). These findings suggest that the temperature variability in our study region is mainly influenced by a combination of AO, NAO, and solar activity.

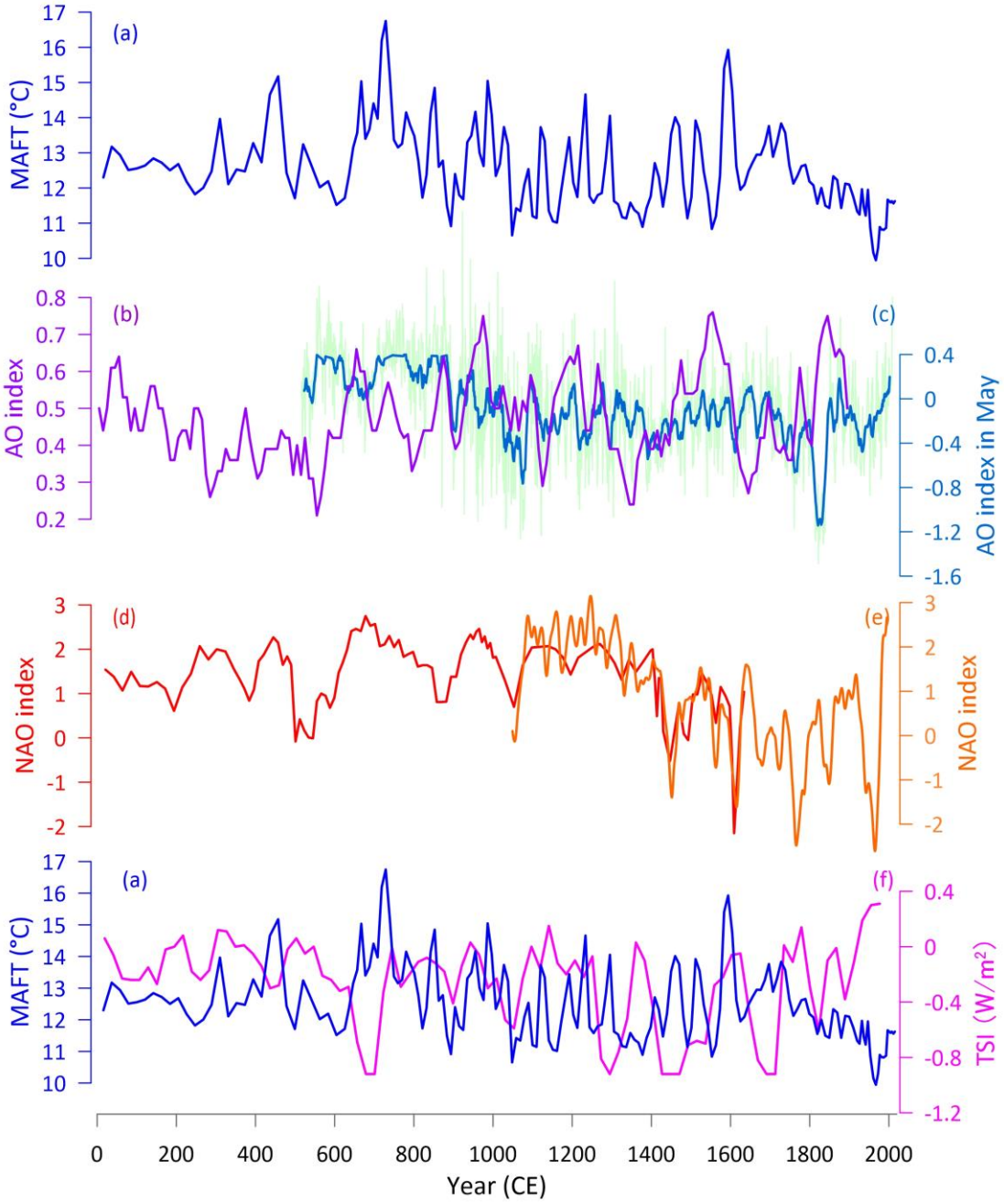

Figure 4. brGDGTs-based temperature variability and climate forcings over the past 2000 years. (a) brGDGT-based MAFTs from Lake Shuanggoushan (this study); (b) 3-point running mean of the AO index inferred from Chinese and Korean historical documents (purple line) (Chu et al., 2008); (c) reconstructed AO index in May from $\delta^{18}O$ tree-ring cellulose (green line) with a 15-point running average (dark blue line) (Sidorova et al., 2021); (d) proxy-derived NAO index from Greenland (red line) (Olsen et al., 2012); (e) annually-resolved reconstructed NAO index from Scotland and Morocco (orange line) (Trouet et al., 2009) (f) reconstructed solar activity (total solar irradiance, W/m^2) from ice cores and tree rings (pink line) (Steinhilber et al., 2012).

4 Conclusions

This study presented a high-resolution temperature reconstruction for the past two millennia of the East Asian monsoon boundary zone in Northeast China. The reconstructed temperatures were based on the brGDGTs from laminated sediments and cross-checked with meteorological data, confirming that they represented the month-above-freezing temperatures between May and October. The temperature reconstruction exhibited decadal-to-centennial variability, with quasi-periodicities of 55-57 and 66-67 years at a 99% confidence level, which may be related to solar activity. Moreover, the temperature fluctuations appeared to be consistent with the trends and magnitudes of the AO/NAO index and solar activity, indicating that the regional temperature variability is influenced by a combination of the AO, NAO, and solar activity. In the future, more quantitative temperature reconstructions and analyses of temperature-driving factors are needed to gain better insights into the mechanisms of temperature evolution.

Acknowledgments

Comments from anonymous reviewers are deeply appreciated. This work was financially supported by the National Natural Science Foundation of China (No.42030507, No.42377206) and the National Research Center for Geoanalysis (CSJ-2022-05).

Data Availability Statement

The supplementary data for this article is available in the open database:

http://doi.org/10.5281/zenodo.10780562

References

Appleby, P. G., Nolan, P. J., Gifford, D. W., Godfrey, M. J., Oldfield, F., Anderson, N. J., et al. (1986). ^{210}Pb dating by low background gamma counting. *Hydrobiologia*, 143, 21-27. doi:10.1007/bf00026640

Büntgen, U., Allen, K., Anchukaitis, K. J., Arseneault, D., Boucher, E., Bräning, A., et al. (2021). The influence of decision-making in tree ring-based climate reconstructions. *Nature Communications*, 12, 3411. doi:10.1038/s41467-021-23627-6

Büntgen, U., Arseneault, D., Boucher, E., Churakova, O. V., Gennaretti, F., Crivellaro, A., et al. (2020). Prominent role of volcanism in Common Era climate variability and human history. *Dendrochronologia*, 64, 125757. doi:10.1016/j.dendro.2020.125757

Cao, J., Rao, Z., Shi, F., & Jia G. (2020). Ice formation on lake surfaces in winter causes warm-season bias of lacustrine brGDGT temperature estimates. *Biogeosciences*, 17, 2521-2536. doi:10.5194/bg-17-2521-2020

Chen, W., & Zhou, Q. (2012). Modulation of the Arctic Oscillation and the East Asian winter climate relationships by the 11-year solar cycle. *Advances in Atmospheric Sciences*, 29(2), 217-226. doi:10.1007/s00376-011-1095-3

Chen, Y., Zheng, F., Yang, H., Yang, W., Wu R., Liu X., et al. (2022). The production of diverse brGDGTs by an Acidobacterium provides a physiological basis for paleoclimate proxies. *Geochimica et Cosmochimica Acta*, 337, 155-165. doi:10.1016/j.gca.2022.08.033

Chu, G., Sun, Q., Wang, X., & Sun, J. (2008). Snow anomaly events from historical documents in eastern China during the past two millennia and implications for low-frequency variability of AO/NAO and PDO. *Geophysical Research Letters*, 35, L14806. doi:10.1029/2008GL034475

Chu, G., Sun, Q., Wang X., Liu, M., Lin, Y., Xie, M. et al. (2011). Seasonal temperature variability during the past 1600 years recorded in historical documents and varved lake sediment profiles from northeastern China. *The Holocene*, 22(7), 785-792. doi:10.1177/0959683611430413

Churakova Sidorova, O. V., Siegwolf, R. T. W., Fonti, M.V. Vaganov, E. A., & Saurer, M. (2021). Spring arctic oscillation as trigger of summer drought in Siberian subarctic over the past 1494 years. *Scientific Reports*, 11, 19010. doi:10.1038/s41598-021-97911-2

Cohen, J., Zhang, X., Francis, J., Jung, T., Kwok, R., Overland, J., et al. (2020). Divergent consensuses on Arctic amplification influence on mid-latitude severe winter weather. *Nature Climate Change*, 10(1), 20–29. doi:10.1038/s41558-019-0662-y

De Jonge, C., Hopmans, E. C., Zell, C. I., Kim, J.-H., Schouten, S., & Sinninghe Damsté J. S. (2014). Occurrence and abundance of 6-methyl branched glycerol dialkyl glycerol tetraethers in soils: Implications for palaeoclimate reconstruction. *Geochimica et Cosmochimica Acta*, 141, 97–112. doi:10.1016/j.gca.2014.06.013

Feng, X., Zhao, C., D'Andrea. W.J., Liang, J., Zhou, A., & Shen, J. (2019). Temperature fluctuations during the Common Era in subtropical southwestern China inferred from brGDGTs in a remote alpine lake. *Earth and Planetary Science Letters*, 510, 26-36. doi:10.1016/j.epsl.2018.12.028

Foster, L. C., Pearson, E. J., Juggins, S., Hodgson, D. A., Saunders, K. M., Verleyen, E., et al. (2016). Development of a regional glycerol dialkyl glycerol tetraether (GDGT)–temperature calibration for Antarctic and sub-Antarctic lakes. *Earth and Planetary Science Letters*, 433, 370–379. doi:10.1016/j.epsl.2015.11.018

Ge, Q., Hao, Z., Zheng, J., & Shao X. (2013). Temperature changes over the past 2000 yr in China and comparison with the Northern Hemisphere. *Climate of the Past*, 9, 1153–1160. doi:10.5194/cp-9-1153-2013

Gong, D., Yang, J., Kim, S. J., Gao, Y., Guo, D., Zhou, T., et al. (2011). Spring Arctic Oscillation-East Asian summer monsoon connection through circulation changes over the western North Pacific. *Climate Dynamics*, 37, 2199–2216. doi:10.1007/s00382-011-1041-1

Halamka, T. A., McFarlin, J. M., Younkin, A. D., Depoy, J., Dildar, N., & Kopf, S. H. (2021). Oxygen limitation can trigger the production of branched GDGTs in culture. *Geochemical Perspectives Letters*, 19, 36-39. doi: 10.7185/geochemlet.2132

He, S., & Wang, H. (2016). Linkage between the East Asian January temperature extremes and the preceding Arctic Oscillation. *International Journal of Climatology*, 36, 1026-1032, doi:10.1002/joc.4399

He, S., GaoY., Li F., Wang H., & He Y. (2017). Impact of Arctic Oscillation on the East Asian climate: A review. *Earth-Science Reviews*, 164: 48–62. doi:10.1016/j.earscirev.2016.10.014

Hegerl, G. C., Crowley, T. J., Hyde, W. T., & Frame, D. J. (2006). Climate sensitivity constrained by temperature reconstructions over the past seven centuries. *Nature*, 440, 1029–1032. doi:10.1038/nature04679

Hu, H.-M., Michel, V., Valensi, P., Mii, H.-S., Starnini, E.,Zunino, M., et al. (2022). Stalagmite-Inferred Climate in the Western Mediterranean during the Roman Warm Period. *Climate*, 10, 93. doi:10.3390/cli10070093

Huth, R., Bochn ́ek, J., & Hejda, P. (2007). The 11-year solar cycle affects the intensity and annularity of the Arctic Oscillation. *Journal of Atmospheric and Solar-Terrestrial Physics*, 69, 1095–1109, doi:10.1016/j.jastp.2007.03.006

Inglis, G.N., Bhattacharya, T., Hemingway, J.D., Hollingsworth, E.H., Feakins, S.J., & Tierney, J.E. (2022). Biomarker approaches for reconstructing terrestrial environmental change. *Annual Review of Earth and Planetary Science*, 50, 369–394. doi:10.1146/annual-earth-032320-095943

436 Jiang, Y., Yuan, X., Zhang, J., Han, S., Chen, Z., Wang, X., et al. (2019). Reconstruction of
437 June-July Temperatures Based on a 233-Year Tree-Ring of *Picea jezoensis* var.
438 *microsperma*. *Forests*, 10, 416, doi:10.3390/f10050416.
439 Knudsen, M. F., Seidenkrantz, M-S., Jacobsen, B. H. & Kuijpers, A. (2011). Tracking the
440 Atlantic Multidecadal Oscillation through the last 8,000 years. *Nature Communication*, 2:
441 178. doi:10.1038/ncomms1186
442 Helama, S., Jones, D. P., & Briffa, K. R. (2017). Dark Ages Cold Period: A literature review and
443 directions for future research. *The Holocene*, 27(10), 1600-1606.
444 doi:10.1177/0959683617693898
445 Land, A., Kromer, B., Remmele, S., Brehm, N., & Wacker, L. (2020). Complex imprint of solar
446 variability on tree rings. *Environmental Research Communications*, 2, 101003.
447 doi:10.1088/2515-7620/abc063
448 Liang, J., Guo, Y., Richter, N., Xie, H., Vachula, R. S., Lupien, R. L., et al. (2022). Calibration
449 and Application of Branched GDGTs to Tibetan Lake Sediments: The Influence of
450 Temperature on the Fall of the Guge Kingdom in Western Tibet, China. *Paleoceanography*
451 *and Paleoclimatology*, 37, e2021PA004393. doi:10.1029/2021PA004393
452 Liu, X., & Ding, R. (2007). The relationship between the Spring Asian Atmospheric circulation
453 and the previous winter Northern Hemisphere annular mode. *Theoretical Applied*
454 *Climatology*, 88, 71–81. doi:10.1007/s00704-006-0231-y
455 Ljungqvist, F. C. (2009). Temperature proxy records covering the last two millennia: a tabular
456 and visual overview. *Geografiska Annaler: Series A, Physical Geography*, 91A, 11–29.
457 doi:10.1111/j.1468-0459.2009.00350.x

458 Loomis, S. E., Russell, J. M., Heureux, A. M., D'Andrea, W. J., & Sinninghe Damsté J. S.
459 (2014). Seasonal variability of branched glycerol dialkyl glycerol tetraethers (brGDGTs) in
460 a temperate lake system. *Geochimica et Cosmochimica Acta*, 144, 173-187.
461 10.1016/j.gca.2014.08.027
462 Mann, M. E., Zhang, Z., Hughes, M. K., Bradley R. S., Miller S. K., Rutherford S., et al. (2008).
463 Proxy-based reconstructions of hemispheric and global surface temperature variations over
464 the past two millennia. *Proceedings of National Academy of Sciences of the United States of*
465 *America*, 105(36). 13252–13257. doi:10.1073/pnas.0805721105
466 Martínez-Sosa, P., Tierney, J. E., Stefanecu, I. C., Crampton-Flood, E. D., Shuman, B N. &
467 Routson, C. (2021). A global Bayesian temperature calibration for lacustrine brGDGTs.
468 *Geochimica et Cosmochimica Acta*, 305, 87-105. doi:10.1016/j.gca.2021.04.038
469 Miller, D. R., Habicht, M. H., Keisling, B. A., Castañeda, I. S. & Bradley, R. S. (2018). A 900-
470 year New England temperature reconstruction from in situ seasonally produced branched
471 glycerol dialkyl glycerol tetraethers (brGDGTs). *Climate of the Past*, 14, 1653-1667.
472 doi:10.5194/cp-14-1653-2018
473 Naafs, B. D. A., Gallego-Sala, A. V., Inglis, G. N., & Pancost, R. D. (2017). Refining the global
474 branched glycerol dialkyl glycerol tetraether (brGDGT) soil temperature calibration.
475 *Organic Geochemistry*, 106, 48-56. doi:10.1016/j.orggeochem.2017.01.009
476 Olsen, J., Anderson, N. J. & Knudsen, M. F. (2012). Variability of the North Atlantic Oscillation
477 over the past 5,200 years. *Nature Geoscience*, 5, 808–812. doi:10.1038/ngeo1589
478 Park, T.-W., Ho, C.-H., & Yang, S., (2011). Relationship between the Arctic Oscillation and cold
479 surges over East Asia. *Journal of Climate*, 24, 68–83. doi:10.1175/2010JCLI3529.1

Qu, W., Li, Y., Li, C., Du L., & Huang, F. (2014). Periodic analysis of solar activity and its link with the arctic oscillation phenomenon. *The Astronomical Journal*, 148, 128, 6. doi:10.1088/0004-6256/148/6/128

Raberg, J. H., Harning, D. J., Crump, S. E., de Wet, G., Blumm, A., Kopf. S., et al. (2021). Revised fractional abundances and warm-season temperatures substantially improve brGDGT calibrations in lake sediments. *Biogeosciences*, 18, 3579–3603. doi:10.5194/bg-18-3579-2021

Reimer, P. J., Austin, W. E. N., Bard, E., Bayliss, A., Blackwell, P. G., Ramsey, C. B., et al. (2020). The Intcal20 Northern Hemisphere Radiocarbon Age Calibration Curve (0–55 cal kBP). *Radiocarbon*, 62(4). 725-757. doi:10.1017/RDC.2020.41

Russell, J. M., Hopmans, E. C., Loomis, S. E., Liang, J., & Sinninghe Damsté J. S. (2018). Distributions of 5- and 6-methyl branched glycerol dialkyl glycerol tetraethers (brGDGTs) in East African lake sediment: Effects of temperature, pH, and new lacustrine paleotemperature calibrations. *Organic Geochemistry*, 117, 56-69. doi:10.1016/j.orggeochem.2017.12.003

Sanchez-Cabeza, J. A., & Ruiz-Fernández, A. C. (2012). ^{210}Pb sediment radiochronology: An integrated formulation and classification of dating models. *Geochimica et Cosmochimica Acta*, 82, 183-200. doi:10.1016/j.gca.2010.12.024

Schouten, S., Hopmans, E. C., & Sinninghe Damsté, J. S. (2013). The organic geochemistry of glycerol dialkyl glycerol tetraether lipids: A review. *Organic Geochemistry*, 54: 19-61. doi:10.1016/j.orggeochem.2012.09.006

Soon, W., Connolly, R., & Connolly, M. (2015). Re-evaluating the role of solar variability on Northern Hemisphere temperature trends since the 19th century. *Earth-Science Reviews*, 150, 409-452. doi: 10.1016/j.earscirev.2015.08.010

Steinhilber, F., Beer, J. & Fröhlich, C. (2009). Total solar irradiance during the Holocene. Geophysical Research Letters 36: L19704. doi:10.1029/2009GL040142

Sun, Q., Chu, G., Liu, M., Xie, M., Li, S., Ling, Y. (2011). Distributions and temperature dependence of branched glycerol dialkyl glycerol tetraethers in recent lacustrine sediments from China and Nepal. *Journal of Geophysical Research*, 116, G01008, doi:10.1029/2010JG001365

Thompson, D. W. J., & Wallace J. M. (1998). The Arctic Oscillation signature in the wintertime geopotential height and temperature fields. *Geophysical Research Letters*, 25, 1297-1300, doi:10.1029/98gl00950

Tourpali, K., Schuurmans, C. J. E., van Dorland, R., Steil. B., Brühl, C., & Manzini, E. (2005). Solar cycle modulation of the Arctic Oscillation in a chemistry-climate model. *Geophysical Research Letters*, 32, 17, L17803, doi:10.1029/2005GL023509

Trouet, V., Esper, J., Graham, N. E., Baker, A., Scourse, J. D., & Frank, D. C. (2009). Persistent positive North Atlantic Oscillation mode dominated the Medieval climate anomaly. *Science*, 2009, 324, 78. doi: 10.1126/science.1166349

Véquaud, P., Thibault, A., Derenne, S., Anquetil, C., Collon, S., Contreras, S., et al. (2022). FROG: A global machine-learning temperature calibration for branched GDGTs in soils and peats. *Geochimica et Cosmochimica Acta*, 318, 468-494. doi:10.1016/j.gca.2021.12.007

Veretenenko, S. V., & Ogurtsov, M. G. (2019). 60-Year Cycle in the Earth's Climate and Dynamics of Correlation Links between Solar Activity and Circulation of the Lower Atmosphere: New Data. *Geomagnetism and Aeronomy*, 59(7), 908-917.

Woo, S.-H., Kim, B.-M., Jeong, J.-H., Kim, S.-J., & Lim, G.-H. (2012). Decadal changes in surface air temperature variability and cold surge characteristics over northeast Asia and their relation with the Arctic Oscillation for the past three decades (1979–2011). *Journal of Geophysical Research*, 117, D18117. doi:10.1029/2011jd016929

Xiao, W., Wang, Y., Zhou, S., Hu, L., Yang, H., et Xu, Y. (2016). Ubiquitous production of branched glycerol dialkyl glycerol tetraethers (brGDGTs) in global marine environments: a new source indicator for brGDGTs. *Biogeosciences*, 13, 5883-5894, doi:10.5194/bg-13-5883-2016

Yao, Y., Wang, L., Huang, Y., Liang, J., Vachula R. S., Cai Y., et al. (2023). Pre-Industrial (1750–1850 CE) Cold Season Warmth in Northeastern China. *Geophysical Research Letters*, 50, e2023GL103591. doi:10.1029/2023GL103591

Zhao, B., Russell, J. M., Tsai, V., Blaus, A., Parish, M., Liang, J., et al. (2023). Evaluating global temperature calibrations for lacustrine branched GDGTs: Seasonal variability, paleoclimate implications, and future directions. *Quaternary Science Reviews*, 310, 108124. doi:10.1016/j.quascirev.2023.108124

Zhu, Z., Wu, J., Rioual, P., Mingram, J., Yang, H., Zhang, B., et al. (2021). Evaluation of the sources and seasonal production of brGDGTs in Lake Sihailongwan (N.E. China) and application to reconstruct paleotemperatures over the period 60-8 ka BP. *Quaternary Science Reviews*, 261, 106946. doi: 10.1016/j.quascirev.2021.106946

544 Zink, K.-G., Vandergoes, M. J., Bauersachs, T., Newnham, R, M., Rees, A. B.H., et Schwark, L.
545 A refined paleotemperature calibration for New Zealand limnic environments using
546 differentiation of branched glycerol dialkyl glycerol tetraether (brGDGT) sources. (2016).
547 *Journal of Quaternary Science*, 31(7), 823-835. doi: 10.1002/jqs.2908